THE JOURNAL OF PHYSICAL CHEMISTRY C

Article

Titanium Nitride Nanoparticles as Plasmonic Solar-Heat Transducers

Satoshi Ishii, Ramu Pasupathi Sugavaneshwar, and Tadaaki Nagao

J. Phys. Chem. C, **Just Accepted Manuscript** • DOI: 10.1021/acs.jpcc.5b09604 • Publication Date (Web): 21 Dec 2015

Titanium Nitride Nanoparticles as Plasmonic Solar-Heat Transducers

Satoshi Ishii,[1,2,*] *Ramu Pasupathi Sugavaneshwar*[1,2] *and Tadaaki Nagao*[1,2]

[1]International Center for Materials Nanoarchitectonics (WPI-MANA), National Institute for Materials Science (NIMS), Tsukuba, Ibaraki 305-0044, Japan

[2]CREST, Japan Science and Technology Agency, Kawaguchi, Saitama 332-0012, Japan

E-mail: sishii@nims.go.jp

Abstract

We demonstrate that lossy plasmonic resonances of nanoparticles are broad enough to cover the majority of solar spectrum and highly efficient for absorbing sunlight. In analytical calculation, we choose a titanium nitride nanoparticle as a lossy plasmonic nano-resonator and present that sunlight absorption efficiency of a titanium nitride nanoparticle is higher than gold and even black carbon nanoparticles. The experiments demonstrate that titanium nitride nanoparticles dispersed in water have high efficiency to heat water and generate vapor than carbon nanoparticles by converting sunlight into heat. Our results open great possibilities for efficient solar heat applications with titanium nitride nanoparticles.

KEYWORDS: nanoparticles; plasmonic resonance; photo-thermal effect; sunlight absorber

Introduction

Efficient usage of solar energy is critically important toward a sustainable society. While solar cells have been gaining a lot of attentions and being considered as a primary method to utilize solar energy, the energy conversion efficiencies of commercial solar cells are 10-20 %[1] and even the state-of-the-art research level solar cells only reach efficiency about 30 %.[2] In contrast, in terms of efficiency, solar water heating systems have much better efficiencies around 40-60 %, which is not yet fully recognized in the society.

In order to take advantage of the solar water heating systems, and further improve their performance, it is necessary to absorb sunlight in a broader spectrum as much as possible ranging from UV to near infrared (NIR). Typically, the surfaces of panels or tubes for solar water heat systems are black to efficiently absorb visible light, and in most cases their absorption ranges extend to NIR. Here the black surfaces are obtained not only from the color of material themselves but also from the surface textures.[3-5] Recently reported nano-textured carbon structures[6-7] are also quite promising in this regard.

Recently nanofluids have gained attention as sunlight absorbers. A nanofluid is a fluid containing nanoparticles (NPs) in which the fluid is not limited but often water. Initially nanofluids have been studied to achieve better thermal conductivities, thus NPs having high thermal conductivities such as alumina NP[8] were chosen. Recently nanofluid has been applied to absorb sunlight, and typical material of choices are carbon-related nanoparticles, such as carbon black[9] and carbon nanotubes[10] and other carbon nano-horns.[11]

Another class of material used in the context of nanofluid is gold.[12-14] Gold NPs are well-known to support localized surface plasmon resonances (LSPRs).[15] It is important in photothermal applications that when gold NPs are at LSPRs both the scattering and absorption are enhanced.[16-18] This phenomenon of plasmon-enhanced light absorption and subsequent local heating has developed into one of the major sub-fields in plasmonics termed as

plasmonic heating or thermo-plasmonics[19] which signifies various photothermal applications in chemistry,[20-21] physics[12] optofluid[22-23] biotechnology[24-25] therapy[26] and imaging.[27-28] Studies have also been done on other metals such as silver, aluminum and copper with respect to thermo-plasmonics.[29-31]

Although plasmon-enhanced absorption of gold NPs is strong, the absorption bandwidth of spherical or cubic-like gold NP is limited to narrow band because the Drude damping factor of gold is small. Various efforts have been made to broaden absorption with gold NPs.[32-33] It has been shown that gold nano-shell structure[14, 34] is useful to broaden light absorption thus could cover majority of solar spectrum.

Towards broadband LSPRs in nanofluids, it is intriguing to look into alternative plasmonic materials other than metals. Note that most of the metals other than noble metals indeed have broadened LSPRs, however, they are easily oxidized and not desirable to be used in water. Among plasmonic ceramics, nitrides[35] and carbides[36-37] have larger damping factors than that of gold and the cross over wavelengths reside in red spectra, thus making them promising candidates to be used as NPs to achieve broadband absorption.[38-39] However, it is not clear whether a plasmonic NP having largest possible damping results in broadband and strong absorption or not.

In the present work, we first elucidate the ideal complex permittivities of NPs to maximize sunlight absorption of NPs in water where the analysis is based on Mie theory.[16] Then we conduct comparative studies of three NPs made of titanium nitride (TiN), carbon and gold by defining a figure of merit. In experiment, we compare the photothermal effects of TiN and carbon nanofluids to pure water under the illumination of a solar simulator. Our analytical calculations and experiments reveal that TiN nanofluid has the highest sunlight absorption properties, even higher than black carbon nanofluid. This result indicates that lossy plasmonic

resonances can indeed have advantage over dielectric NPs having broadband losses. Our work opens another application of TiN as efficient sunlight absorber in the form of nanofluid.

Analytical calculation

In general, a material with larger Im[ε] tends to absorb more light where ε denotes complex permittivity. With regard to a nanosphere (NS), interaction of light by a NS can be fully expressed by Mie theory.[16] Note the NPs we used in the experiments were not spherical, however, they are highly symmetric and the analysis considering spheres qualitatively holds true for our NPs. Absorption cross section which is calculated from Mie theory is a measure of the probability of photon absorption by a sphere. It is often convenient to introduce absorption efficiency where absorption cross section is divided by the cross section of a sphere. An absorption efficiency ($Q_{abs}(x, m)$) is a function of x and m, where size parameter x (= kr) is given by the multiple of the wavenumber (k) and the particle radius (r) and m is the relative refractive index of the sphere normalized by the host index. For a non-magnetic material, the permeability is unity thus the refractive index is the square root of the permittivity.

To find out the complex permittivity to maximize the Q_{abs} of a NS, we plot Q_{abs} in Im[ε] - Re[ε] space for three different size parameters, x = 0.3, 0.5 and 0.7 as shown in Figure 1(a-c) where the calculation is based on Mie theory. The host is assumed to be water whose refractive index is 1.33 in optical range. For instance, the size parameters take 0.3, 0.5 and 0.7 when the incident wavelengths are 1047 nm, 628 nm and 449 nm, respectively, for a sphere of 50 nm in radius. In each figure, there is an area where Q_{abs} is enhanced and the value becomes larger than unity. This enhancement is due to LSPRs of a NS. Note that too large Im[ε] decreases Q_{abs} value from the maximum.

From Figure 1(a-c), if one wants to have broad absorption with a nanofluid, it is desirable to search for a material having |Re[ε]| as well as Im[ε] on the order of unity for broad spectral range. Based on these analysis, we then chose three materials, gold,[40] titanium nitride[41] and amorphous carbon[42] for comparison. As gold is one of the two most widely used plasmonic materials, TiN is a highly conductive metallic ceramic and carbon is a typical material which appears black. The interpolated permittivites of the three materials taken from the reference data are plotted in Figure 1(d). Each permittivity is shown from 300 nm to 1400 nm in wavelength. Within the plotted wavelength range, gold is highly dispersive. The difference between TiN and carbon lies in Re[ε] where $\mathrm{Re}[\varepsilon_{TiN}]$ is negative beyond ~500 nm, however, $\mathrm{Re}[\varepsilon_{C}]$ is positive within the plotted range. Among the three materials, the permittivity curve of TiN in Figure 1(d) stays in the high-Q_{abs} areas in Figure 1(a-c),

Using the identical permittivity data as Figure 1(d), in Figure 1(e) we plot the absorption efficiencies of spheres of 50nm in radius. The absorption efficiency of a gold NS shows a sharp peak at ~530 nm which is due to LSPRs. Carbon NS shows broad absorption as can be expected from its black color. It is interesting to look at the absorption efficiency of a TiN NS; it has a LSPR peak similar to a gold NS, however the peak is broader than that of gold NS, thus the absorption range is similar to that of carbon NS. The area plot superimposed in Figure 1(e) is the normalized AM1.5G spectrum. Among the three materials, the curve for TiN NS overlaps the most to the AM1.5G plot.

To quantitatively evaluate the sunlight absorption efficiency of a nanoparticle in water, we define the figure of merit (FoM) by multiplying the absorption efficiency of a NS and normalized AM1.5G (E) and integrate over the wavelength from 300 nm to 1400 nm, as shown in Eq. (1). The integral is up to 1400 nm because the water, which is the host fluid in our case, absorbs significantly beyond ~1400 nm.

$$FoM = \int_{300}^{1400} Q_{\mathrm{abs}}(\lambda)E(\lambda)d\lambda \qquad (1)$$

The FoMs of NSs with 50 nm in radius are plotted in Figure 1(f). The FoM of a TiN NS is the highest among the three NSs, which is nearly twice the value of that of a carbon NS. Therefore, TiN nanofluid is expect to absorb sunlight effectively.

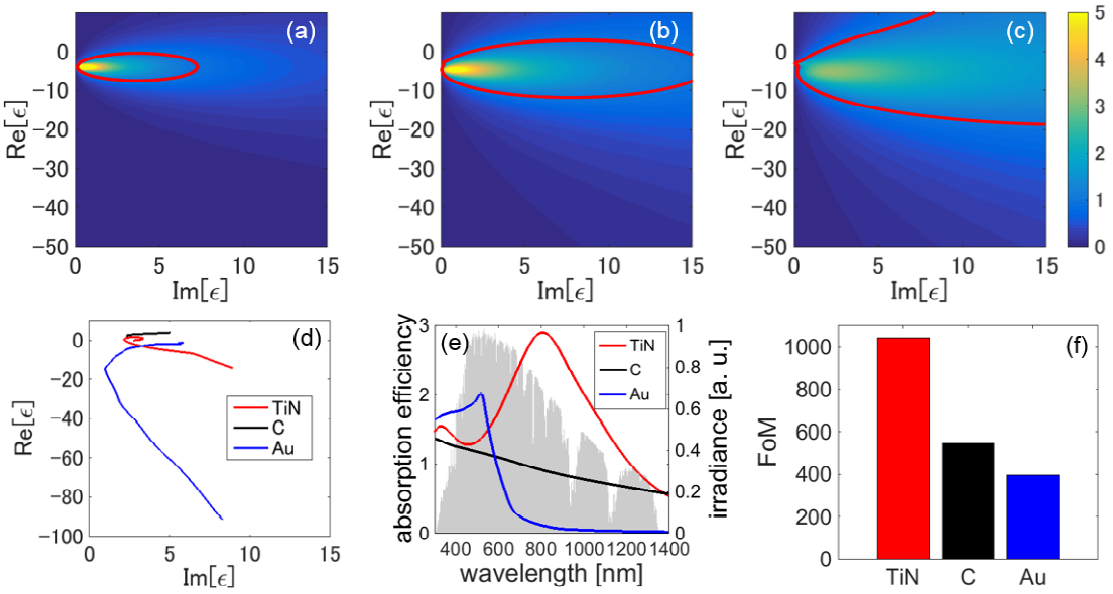

Figure 1. (a-c) Calculated absorption efficiencies of NSs with 100 nm in diameter where the host is water (n = 1.33). Red contours in each panel are for Q_{abs} = 1. (a) x = 0.3, (b) = 0.5, (c) = 0.7. (d) Complex permittivities of TiN, carbon and Au from 300 nm to 1400 nm plotted in Re[ε] vs. Im[ε] space. (e) Calculated absorption efficiencies of NSs in water made of TiN, carbon and Au where the radii are 50 nm. The area plot in grey color shows the normalized irradiance of AM1.5G. (f) Figure-of-merits for NSs with 50-nm radius in water made of TiN, carbon and Au.

Experimental

In experiment, we selected TiN and carbon NPs which showed higher FoMs and are promising to absorb sunlight broadly. The TiN NPs were synthesized through the thermal plasma processing.[43] Briefly, the source material was vaporized in RF thermal plasma at ~10,000 K and quenched to form NPs. Carbon black (#30) synthesized by the furnace method were purchased from Mitsubishi Chemicals.

For the sunlight heating experiments, each nanoparticle was dispersed into 20 ml of pure water and sonicated for a few minutes. No surfactants were used as both of the NPs were dispersed well and did not produce visible aggregations which sank under water.

A solar simulator (XES-40S1, San-Ei Electric) was used to evaluate the solar heating properties of the nanofluids. Due to the limitation of the experimental setting, the irradiance was fixed to 80 mW/cm^2 in all the measurements shown in Figure 3, which was the highest irradiance achievable without focusing. Only at the experiment to show visible vapor, a Fresnel lens used to focus the light. The weight and temperature changes were monitored by an electric balance (AUW220D, Shimadzu) and a type K thermo-couple, respectively. When monitoring weight and temperature under light illumination, each solution was kept in a glass beaker which was surrounded by a white cup made of polystyrene foam for thermal isolation. The top of the beaker was left open so that vapor can go out. During the measurements, the room temperature and humidity were kept at 19~20 °C and 36~43 %, respectively.

Results and discussion

The TEM images of the TiN and carbon NPs are shown in Figure 2(a) and 2(b), respectively. From the TEM images, the size of the single TiN and carbon NPs are ~30 nm and ~40 nm, respectively, however, the measurement from dynamic light scattering (DLS) showed the average sizes of TiN and carbon NPs in water were 132 nm and 127 nm, respectively (see Figure S1, Supporting Information). These results suggest that several NPs could have aggregated in water for both of the NPs which in turn could have led to higher measured values in DLS.

The XRD patterns plotted in Figure 2(c) show a single phase of TiN for TiN NPs and amorphous phase for carbon NPs. High-resolution TEM images shown in Figure S2 (Supporting Information) verify the crystalline phase for TiN NPs and amorphous phase for carbon NPs.

Figure 2(d) shows the absorbance of TiN and carbon NPs dispersed in water. Note that absorbance contains scattered light in addition to absorbed light. At the identical volume

concentration (vol%), the absorbance of the TiN NPs was higher than that of the carbon NPs from UV to NIR. The broad peak at 700 nm for TiN NPs is due to the lossy plasmon resonances. As scattering also contributes to efficient light trapping,[44] the results indicate that TiN nanofluid has the potential to harvest sunlight much more than carbon nanofluid.

In order to identify the peak at 700 nm for TiN NPs, we numerically calculated absorption (resistive heating) for a TiN NP and a carbon NP as shown in Figure 2(e) and 2(f), respectively. At 700 nm, the absorption of the TiN NP is clearly higher than that of the carbon NP due to lossy plasmon resonances, thus supporting the experiment.

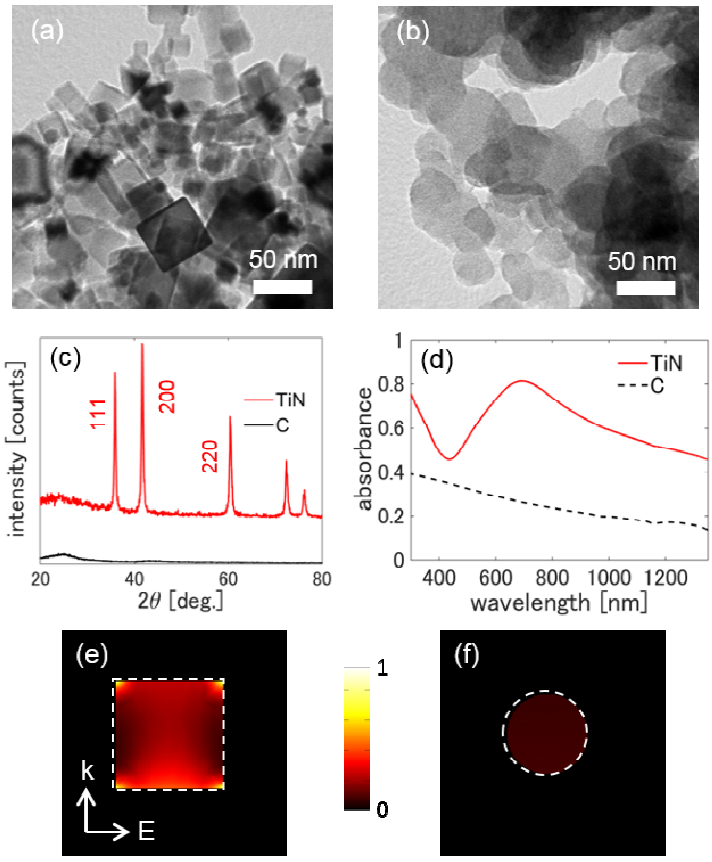

Figure 2. (a, b) Bright-field TEM images of TiN NPs (a) and carbon NPs (b). (c) X-ray diffraction patterns of TiN and carbon NPs. (d) Absorbance of TiN and carbon nanofluids at 0.001 vol% each. (e-f) Numerically evaluated absorption (resistive heating) of a 40-nm TiN NP (e) and a 30-nm carbon NP (f) eilluminated at 700 nm.

Next we provide a proof of concept demonstration that TiN nanofluid has high performance in absorbing sunlight to rise the temperature of the fluid and vaporize water. Figure 3 shows

the weight changes and temperature changes of the TiN and carbon nanofluids under the illumination of a solar simulator at 80 mW/cm^2. From Figure 3(a) and 3(b), the higher the concentration is, the faster the water vaporizes for both of the nanofluids. When the two nanofluids are compared at the same volume concentration, the TiN nanofluid always vaporizes more than that of the carbon nanofluid. Thus, the TiN NPs generate solar vapor much efficiently than the carbon NPs. With regard to the temperature rises as shown in Figure 3(c-d), both TiN and carbon nanofluids have better light-to-heat conversion than pure water. However, from Figure 3(c-d) the highest temperature after 1200 seconds of illumination was the nanofluid at 0.001 vol% and gradually deceased as the concentrations get higher. Such trend is prominently seen for carbon nanofluids. It could be the case that at higher concentrations absorbed solar energy is tend to be consumed for vapor generation rather than heating the nanofluids. The reason is still not clear and further analysis is in progress. When compared at the identical concentrations, TiN nanofluids were heated up to higher temperatures than carbon nanofluids. From these results, it could be seen that TiN nanofluids have better vapor generation and heating properties than carbon nanofluids and the differences are more distinct at lower concentrations. At higher concentration, multiple absorptions compensate the lower absorption efficiency of carbon NPs, which made the difference smaller.

Additionally, to visualize vapor generation, 0.1 vol% TiN nanofluid was irradiated by focused light from the solar simulator (800 mW/cm^2). The photo of the nanofluid under illumination is presented in Figure S3 (Supporting Information). Although the temperature of the TiN nanofluid at the bottom was ~29 °C, solar generated steam is clearly seen, which proves the efficient local heating of the TiN nanoparticles by lossy plasmonic resonances.

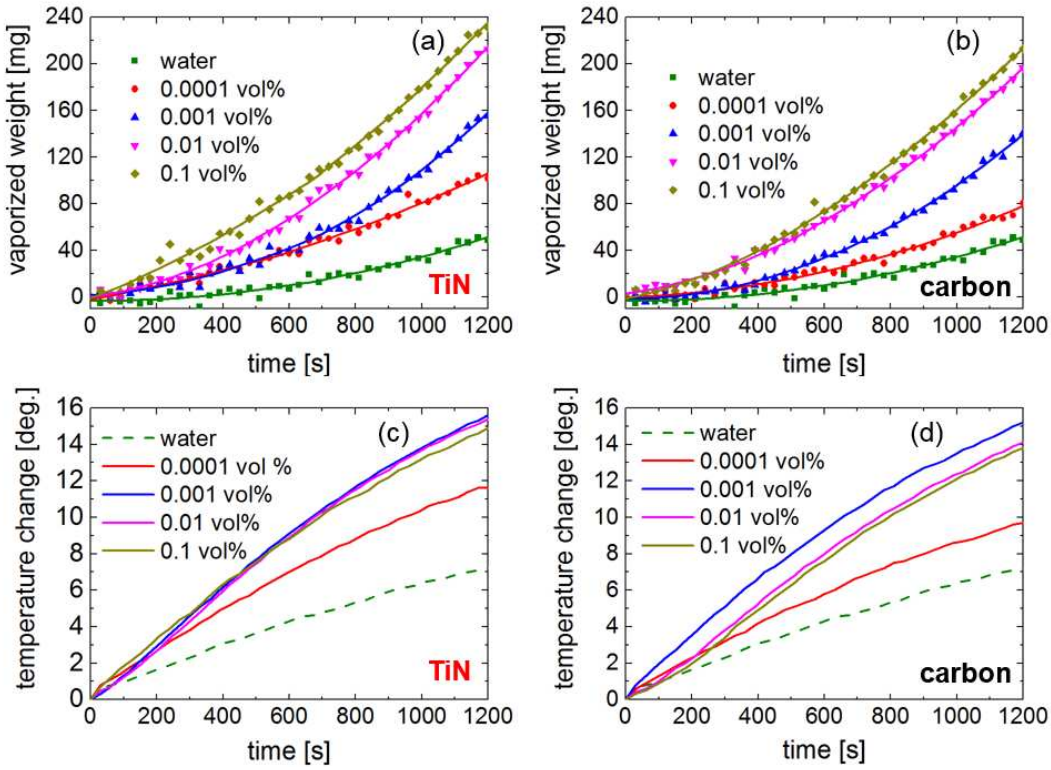

Figure 3. (a-b) Weight changes due to vaporization upon sunlight illumination for (a) TiN and (b) carbon nanofluids at different concentrations. The sold lines are the fitted plots to the experimental data plotted in symbols. (c-d) Temperature changes upon sunlight illumination for (c) TiN and (d) carbon nanofluids at different concentrations.

In Figure 3, we see that the nanofluids at higher concentrations vaporize water faster. Since the temperatures of nanofluids are higher than that of water, one could consider that increased vaporization could be the outcome of increased nanofluid temperatures. To resolve the temperature effect, the illumination intensities for TiN nanofluid and carbon nanofluid were lowered at 43 mW/cm^2 to keep the equilibrium temperature of TiN nanofluid, carbon nanofluid and water at the constant temperatures. The results are plotted in Figure 4 where the concentrations of TiN and carbon nanofluids in Figure 4(a) and 4(b) are 0.001 vol% and 0.01 vol%, respectively. The results clearly show that even at identical temperatures, the nanofluids have higher vaporization speed and TiN nanofluids vaporized itself more than carbon nanofluid. Therefore, the NPs in the nanofluids enhance the vaporization speed by

concentrating sunlight in nano-scale and TiN NPs is superior to carbon NPs in terms of generating solar vapor.

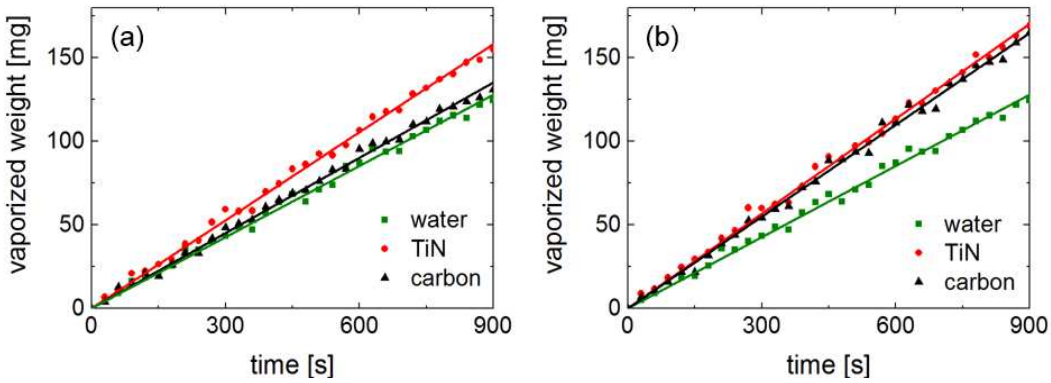

Figure 4. Weight change by vaporization kept at the constant temperature. The illumination power for water and the two nanofluids were adjusted such that after ~1 hour the temperatures became equilibrium and all the temperature were at 33.4±0.3 °C. The concentrations of TiN and carbon nanofluids in panel (a) and (b) are 0.001 vol% and 0.01 vol%, respectively. The solid lines are the linear fittings to the experimental data.

Our study has demonstrated that TiN nanofluid is promising for solar heat applications. TiN can used for an application in solar water heating system in the following ways, heated TiN nanofluid can go through a heat exchanger to heat tap water for drinking, washing or showering. Similarly, heated TiN nanofluid can be used with a heat-pump for an air conditioner. Furthermore, in contrast to the current solar water heating system, the use of TiN nanofluid eliminate the need of black tubes or panels for sunlight absorber, which is favorable for the following reasons. While water is indirectly heated through the absorber for conventional system, water is directly heated by TiN NPs for the present nanofluid system, thus the heat losses can be reduced. At the same time, the heat capacitance of NPs are negligibly small compared to that of tubes or panels, thus reducing the extra thermal capacitance of the system.

Also the enhanced vaporization property of TiN nanofluid could be useful in getting clean water from contaminated water or sea water. TiN NPs are not consumed during vapor generation, so a nanofluid-base water supplying system can work for a long time, which

makes it beneficial in the case of emergencies or for the usages in developing countries. It should be noted that solar vapor generation reported by others used focused sunlight,[6, 14] hence the vaporization speed were faster than our results.

In our current work, we only studied TiN as a material which meets the criteria shown in Figure 1. Yet, as briefly mentioned earlier, there are other candidates other than TiN. Zirconium nitride, hafnium nitride are some of the other nitrides which have similar dielectric functions to that of TiN.[35] Zirconium carbide[37] and tantalum carbide[36] have also similar dielectric functions as well. Borides can be another class of materials which can be used.[42] It is anticipated that these materials can be also used for solar heat applications.

Conclusions

To summarize, we demonstrated that lossy plasmonic resonances in nanofluids are useful towards enhancing sunlight absorption. For the purpose of qualitatively screening NP materials, we introduced the FoM as an integral of absorption efficiency and normalized solar irradiance and showed that TiN NP takes higher FoM than gold and carbon nanoparticles. The experimental data showed that TiN nanofluid has better sunlight absorption properties to generate solar vapor and heat water than pure water, even better than carbon nanofluid when compared at the same concentrations. Solar water heating in nanofluid is direct and does not require any sunlight absorbers, thus the improvement in efficiency is expected. Another feature of TiN nanofluid is that it vaporizes faster than pure water even at the identical temperatures, which is advantageous for getting distilled water. Further studies on nanofluid will pave a way toward efficient solar water heating systems and solar distillation systems.

Methods on analytical and numerical calculations

The numerical calculation was based on Mie theory which was coded in MALAB. In the calculation, the material properties were exported from the references cited in the main text. The numerical calculations were done using COMSOL which is a commercial software based on finite element method. The solution was solved for the scattered field and the host material was set to water whose refractive index is 1.33. The incident field was a linearly polarized plane wave propagating from the bottom to top at 700 nm in wavelength. The TiN NP and carbon NP were modeled as a cube and a sphere, respectively.

Acknowledgements

This work is in part supported by the JSPS KAKENHI Grant Number 15K17447. The authors would like to thank Nisshin Engineering Inc. for the TiN NP synthesis, S. Horii for fruitful discussions and MANA Technical Support Team for their technical supports.

Supporting Information

Supporting Information is available online.

References

1. *Renewable Energy Cost Analysis - Solar Photovoltaics*; IRENA: IRENA working paper, 2012.
2. Green, M. A.; Emery, K.; Hishikawa, Y.; Warta, W.; Dunlop, E. D., Solar Cell Efficiency Tables (Version 45). *Prog. Photovoltaics* **2015**, *23*, 1-9.
3. Jansen, H.; de Boer, M.; Legtenberg, R.; Elwenspoek, M., The Black Silicon Method: A Universal Method for Determining the Parameter Setting of a Fluorine-Based Reactive Ion Etcher in Deep Silicon Trench Etching with Profile Control. *J. Micromech. Microeng.* **1995**, *5*, 115.
4. Xu, Z.; Chen, Y.; Gartia, M. R.; Jiang, J.; Liu, G. L., Surface Plasmon Enhanced Broadband Spectrophotometry on Black Silver Substrates. *Appl. Phys. Lett.* **2011**, *98*, 241904.
5. Theocharous, E.; Chunnilall, C. J.; Mole, R.; Gibbs, D.; Fox, N.; Shang, N.; Howlett, G.; Jensen, B.; Taylor, R.; Reveles, J. R., The Partial Space Qualification of a Vertically Aligned Carbon Nanotube Coating on Aluminium Substrates for Eo Applications. *Opt. Express* **2014**, *22*, 7290-7307.
6. Ghasemi, H.; Ni, G.; Marconnet, A. M.; Loomis, J.; Yerci, S.; Miljkovic, N.; Chen, G., Solar Steam Generation by Heat Localization. *Nat. Commun.* **2014**, *5*.

7. Ito, Y.; Tanabe, Y.; Han, J.; Fujita, T.; Tanigaki, K.; Chen, M., Multifunctional Porous Graphene for High-Efficiency Steam Generation by Heat Localization. *Adv. Mater.* **2015**, *27*, 4302-4307.
8. Masuda, H.; Ebata, A.; Teramae, K.; Hishinuma, N., Alteration of Thermal Conductivity and Viscosity of Liquid by Dispersing Ultra-Fine Particles. *Netsu Bussei* **1993**, *7*, 227-233.
9. Han, D.; Meng, Z.; Wu, D.; Zhang, C.; Zhu, H., Thermal Properties of Carbon Black Aqueous Nanofluids for Solar Absorption. *Nanoscale Res. Lett.* **2011**, *6*, 1-7.
10. Hordy, N.; Rabilloud, D.; Meunier, J.-L.; Coulombe, S., High Temperature and Long-Term Stability of Carbon Nanotube Nanofluids for Direct Absorption Solar Thermal Collectors. *Sol. Energy* **2014**, *105*, 82-90.
11. Mercatelli, L.; Sani, E.; Zaccanti, G.; Martelli, F.; Di Ninni, P.; Barison, S.; Pagura, C.; Agresti, F.; Jafrancesco, D., Absorption and Scattering Properties of Carbon Nanohorn-Based Nanofluids for Direct Sunlight Absorbers. *Nanoscale Res. Lett.* **2011**, *6*, 1-9.
12. Lukianova-Hleb, E. Y.; Lapotko, D. O., Influence of Transient Environmental Photothermal Effects on Optical Scattering by Gold Nanoparticles. *Nano Lett.* **2009**, *9*, 2160-2166.
13. Lapotko, D., Plasmonic Nanoparticle-Generated Photothermal Bubbles and Their Biomedical Applications. *Nanomedicine* **2009**, *4*, 813-845.
14. Neumann, O.; Urban, A. S.; Day, J.; Lal, S.; Nordlander, P.; Halas, N. J., Solar Vapor Generation Enabled by Nanoparticles. *ACS Nano* **2012**, *7*, 42-49.
15. Craighead, H.; Niklasson, G., Characterization and Optical Properties of Arrays of Small Gold Particles. *Appl. Phys. Lett.* **1984**, *44*, 1134-1136.
16. Bohren, C. F.; Huffman, D. R., *Absorption and Scattering of Light by Small Particles*; John Wiley & Sons, 2008.
17. Cole, J. R.; Mirin, N. A.; Knight, M. W.; Goodrich, G. P.; Halas, N. J., Photothermal Efficiencies of Nanoshells and Nanorods for Clinical Therapeutic Applications. *J. Phys. Chem. C* **2009**, *113*, 12090-12094.
18. Chen, H.; Shao, L.; Ming, T.; Sun, Z.; Zhao, C.; Yang, B.; Wang, J., Understanding the Photothermal Conversion Efficiency of Gold Nanocrystals. *Small* **2010**, *6*, 2272-2280.
19. Baffou, G.; Quidant, R., Thermo‐Plasmonics: Using Metallic Nanostructures as Nano‐Sources of Heat. *Laser Photonics Rev.* **2013**, *7*, 171-187.
20. Xiao, M.; Jiang, R.; Wang, F.; Fang, C.; Wang, J.; Yu, J. C., Plasmon-Enhanced Chemical Reactions. *Journal of Materials Chemistry A* **2013**, *1*, 5790-5805.
21. Cao, L.; Barsic, D. N.; Guichard, A. R.; Brongersma, M. L., Plasmon-Assisted Local Temperature Control to Pattern Individual Semiconductor Nanowires and Carbon Nanotubes. *Nano Lett.* **2007**, *7*, 3523-3527.
22. Farahi, R.; Passian, A.; Ferrell, T.; Thundat, T., Marangoni Forces Created by Surface Plasmon Decay. *Opt. Lett.* **2005**, *30*, 616-618.
23. Donner, J. S.; Baffou, G.; McCloskey, D.; Quidant, R., Plasmon-Assisted Optofluidics. *ACS Nano* **2011**, *5*, 5457-5462.
24. Han, G.; Ghosh, P.; De, M.; Rotello, V. M., Drug and Gene Delivery Using Gold Nanoparticles. *Nanobiotechnology* **2007**, *3*, 40-45.
25. Ghosh, P.; Han, G.; De, M.; Kim, C. K.; Rotello, V. M., Gold Nanoparticles in Delivery Applications. *Adv. Drug Delivery Rev.* **2008**, *60*, 1307-1315.
26. Loo, C.; Lin, A.; Hirsch, L.; Lee, M.-H.; Barton, J.; Halas, N.; West, J.; Drezek, R., Nanoshell-Enabled Photonics-Based Imaging and Therapy of Cancer. *Technology in cancer research & treatment* **2004**, *3*, 33-40.
27. Boyer, D.; Tamarat, P.; Maali, A.; Lounis, B.; Orrit, M., Photothermal Imaging of Nanometer-Sized Metal Particles among Scatterers. *Science* **2002**, *297*, 1160-1163.

28. Cognet, L.; Tardin, C.; Boyer, D.; Choquet, D.; Tamarat, P.; Lounis, B., Single Metallic Nanoparticle Imaging for Protein Detection in Cells. *Proc. Natl. Acad. Sci.* **2003**, *100*, 11350-11355.
29. Taylor, R. A.; Phelan, P. E.; Otanicar, T.; Adrian, R. J.; Prasher, R. S., Vapor Generation in a Nanoparticle Liquid Suspension Using a Focused, Continuous Laser. *Appl. Phys. Lett.* **2009**, *95*, 161907.
30. Taylor, R. A.; Phelan, P. E.; Otanicar, T. P.; Walker, C. A.; Nguyen, M.; Trimble, S.; Prasher, R., Applicability of Nanofluids in High Flux Solar Collectors. *J. Renewable Sustainable Energy* **2011**, *3*, 023104.
31. Li, Y.; Verbiest, T.; Strobbe, R.; Vankelecom, I. F. J., Silver Nanoparticles as Localized "Nano-Heaters" under Led Light Irradiation to Improve Membrane Performance. *Journal of Materials Chemistry A* **2014**, *2*, 3182-3189.
32. Payne, E. K.; Shuford, K. L.; Park, S.; Schatz, G. C.; Mirkin, C. A., Multipole Plasmon Resonances in Gold Nanorods. *Journal of Physical Chemistry B* **2006**, *110*, 2150-2154.
33. Liu, L.; Dao, T. D.; Kodiyath, R.; Kang, Q.; Abe, H.; Nagao, T.; Ye, J., Plasmonic Janus‐Composite Photocatalyst Comprising Au and C‐Tio2 for Enhanced Aerobic Oxidation over a Broad Visible‐Light Range. *Adv. Funct. Mater.* **2014**, *24*, 7754-7762.
34. Neumann, O., et al., Compact Solar Autoclave Based on Steam Generation Using Broadband Light-Harvesting Nanoparticles. *Proc. Natl. Acad. Sci.* **2013**, *110*, 11677-11681.
35. Naik, G. V.; Shalaev, V. M.; Boltasseva, A., Alternative Plasmonic Materials: Beyond Gold and Silver. *Adv. Mater.* **2013**, *25*, 3264-3294.
36. Modine, F.; Major, R.; Haywood, T.; Gruzalski, G.; Smith, D., Optical Properties of Tantalum Carbide from the Infrared to the near Ultraviolet. *Phys. Rev. B* **1984**, *29*, 836.
37. Modine, F.; Haywood, T.; Allison, C., Optical and Electrical Properties of Single-Crystalline Zirconium Carbide. *Phys. Rev. B* **1985**, *32*, 7743.
38. Guler, U.; Naik, G. V.; Boltasseva, A.; Shalaev, V. M.; Kildishev, A. V., Performance Analysis of Nitride Alternative Plasmonic Materials for Localized Surface Plasmon Applications. *Appl. Phys. B* **2012**, *107*, 285-291.
39. Guler, U.; Suslov, S.; Kildishev, A. V.; Boltasseva, A.; Shalaev, V. M., Colloidal Plasmonic Titanium Nitride Nanoparticles: Properties and Applications. *arXiv preprint arXiv:1410.3920* **2014**.
40. Johnson, P. B.; Christy, R.-W., Optical Constants of the Noble Metals. *Phys. Rev. B* **1972**, *6*, 4370-4379.
41. Naik, G. V.; Schroeder, J. L.; Ni, X.; Kildishev, A. V.; Sands, T. D.; Boltasseva, A., Titanium Nitride as a Plasmonic Material for Visible and near-Infrared Wavelengths. *Opt. Mater. Express* **2012**, *2*, 478-489.
42. Palik, E. D., *Handbook of Optical Constants of Solids*; Academic press, 1998; Vol. 3.
43. Nakamura, K., Synthesis of Nanoparticles by Thermal Plasma Processing and Its Applications *Earozoru Kenkyu* **2014**, *29*, 98-103.
44. Hogan, N. J.; Urban, A. S.; Ayala-Orozco, C.; Pimpinelli, A.; Nordlander, P.; Halas, N. J., Nanoparticles Heat through Light Localization. *Nano Lett.* **2014**, *14*, 4640-4645.

Table of Contents (TOC)